Grousers Effect in Tracked Vehicle Multibody Dynamics with Deformable Terrain Contact Model

applied sciences

MDPI

Article

Grousers Effect in Tracked Vehicle Multibody Dynamics with Deformable Terrain Contact Model

Francesco Mocera *,†, **Aurelio Somà** † **and Andrea Nicolini** †

Department of Mechanical and Aerospace Engineering—Politecnico di Torino, Corso duca degli Abruzzi 24, 10129 Torino, Italy; aurelio.soma@polito.it (A.S.); andrea.nicolini@polito.it (A.N.)

* Correspondence: francesco.mocera@polito.it

† These authors contributed equally to this work.

Received: 4 August 2020; Accepted: 27 August 2020; Published: 21 September 2020

Abstract: In this work, a multibody model of a small size farming tracked vehicle is shown. Detailed models of each track were coupled with the rigid body model of the vehicle. To describe the interaction between the track and the ground in case of deformable soil, custom defined forces were applied on each link of the track model. Their definition derived from deformable soil mechanics equations implemented with a specifically designed routine within the multibody code. According to the proposed model, it is assumed that the main terrain deformation is concentrated around the vehicle tracks elements. The custom defined forces included also the effects of the track grousers which strongly affect the traction availability for the vehicle. A passive soil failure model was considered to describe the terrain behaviour subjected to the grousers action. A so developed model in a multibody code can investigate vehicle performance and limit operating conditions related to the vehicle and soil characteristics. In this work, particular attention was focused on the results in terms of traction force, slip and sinkage on different types of terrain. Tests performed in the multibody environment show how the proposed model is able to obtain tractive performance similar to equivalent analytical solutions and how the grousers improve the availability of tractive force for certain type of soil characteristics.

Keywords: deformable soil; tracked vehicle; multibody; contact model

1. Introduction

Numerical simulations are very useful tools to evaluate complex mechanical systems behaviour during their early design stage as well as during product development. Multibody models are widely used to predict vehicle kinematics and dynamics [1], giving the ability to identify/predict safety critical working conditions to be avoided [2,3]. Focusing on wheeled or tracked vehicles, machine-soil contact modelling is relevant to assess its performance. Several mathematical models have been proposed in the literature to characterize wheel or track-terrain interaction [4,5].

A comprehensive contact model is a particularly complex task to be accomplished. The identification of the terrain mechanical characteristics is strongly affected by its composition and humidity content. A terrain can be described as an elasto-plastic medium which exhibits a strong non-linearity in the force-deformation characteristic. The behaviour of different types of soil has been characterized by means of several empirical parameters for terrain cohesion, internal friction angle and stiffness [6–8]. Several numerical models have been proposed in the literature to study and simulate wheel-soil interaction [9–11] as well as the experimental test rigs to characterize them [12]. Similarly, empirical methods, discrete elements and finite elements methods as well as reduced order models have been proposed to model the terrain-tyre and terrain track interaction response when in contact with machines wheels or tracks modelled as rigid or flexible bodies [13–15]. Two mathematical models

are usually considered to represent the track(or wheel)-soil interaction—the Bekker's model and the Janosi-Hanamoto's law. Bekker's equation relates the normal pressure exerted on the ground with the vertical sinkage of a circular or rectangular plate used for the soil characterization procedure through a non-linear elastic relationship. When modelling the sinkage behaviour of the tracked machine also the soil damping contribution should be considered.Janosi-Hanamoto equation relates shear stress to the corresponding shear displacement of the soil. The difference between the actual shear stress and the maximum one admissible by the terrain strongly affects the availability of tractive force to be developed by the tracked vehicle. Both the models depend on empirical parameters to be derived through specific terrain characterization procedures [16]. A novel soil-tyre model has been recently proposed in Reference [17] integrating soil mechanics behaviour with a soft soil-elastic tyre interaction model. The tyre and soil deformations are computed iteratively solving the equilibrium problem as implemented by Sharaf et al. in Reference [18] to model an off-road vehicle. On the other hand, different procedures have been adopted to model a deformable terrain in multibody (MTB) codes. Rubinstein and Hitron [19] modelled the terrain shape with rigid bodies whereas in other MTB codes discrete elements method (DEM), finite element or mesh free methods [20] have been proposed. A springs-damper-oil sand slots connected by spherical joints terrain modelling approach was proposed by Frimpong and Thiruvengadam [21,22]. Soil modelling through triangular meshes or discrete elements was also considered in the Adams Tracked Vehicle Toolkit (ATV) [20,23,24]. In other numerical environments, soil behaviour under load has also been investigated thanks to Finite Element Models (FEMs) [25] or Semi-empirical Contact Models (SCMs) [26]. There are two different types of tracks classified as rigid or flexible. Rubber tracks, reinforced with a steel core, are usually classified as flexible whereas tracks made of steel links are classified as rigid. The latter are composed of rigid links [27] usually connected in multibody models with rotational joints [28] or bushing elements [29]. Bushing elements can also damp the system to limit numerical errors [30]. In fact, simple rotational joints without damping can lead to high vibration phenomena of the track links [31].

In this paper a MTB model of a tracked machine with a deformable terrain model was developed, also thanks to the authors' research group previous experience in MTB contact [32] and vehicle modelling [33]. The main assumption of the model considers the terrain deformation located in a close area around the vehicle tracks. Thus, the soil deformation can be kinematically correlated to the track motion. The soil mechanics equations were implemented on each rigid body used to model the rubber tracks. Each link is connected to each contiguous one by means of bushing elements aimed to replicate a realistic track elastic characteristic. Soil mechanics equations were implemented through a specifically designed routine which solved only the equations for the track links in contact with the terrain. The algorithm defined at each iteration the forces applied to each track link in contact with the terrain. Moreover, the effects of grousers in the overall tractive performance of the machine were investigated. To model grousers effects, soil mechanics equations related to passive terrain failure [34,35] were considered and machine draw-bar pull was evaluated for different types of soil.

2. Soil Mechanics

In this section, the soil mechanics equations implemented in the multibody environment are summarized. The soil behaviour when compressed in normal direction can be described with the Bekker equation (Equation (1)), also known as the pressure-sinkage relationship [6].

$$p = \left(\frac{k_c}{b} + k_\phi\right) \cdot y^n = k_{eq} \cdot y^n, \tag{1}$$

with y representing the sinkage coordinate while k_c, k_ϕ are empirical coefficients describing the cohesion and the internal friction angle of the considered type of soil. n is the sinkage exponent and b the reference dimension of a circular or rectangular plate in contact with the terrain. A different formulation of Bekker law was proposed by Reece in Reference [16]. Wong et al. [11] formulated a pressure-sinkage relationship describing also the soil response during an unloading cycle or when

pressure removal occurs. The soil shear stress-shear displacement relationship in the longitudinal direction of the track can be described trough the Janosi-Hanamoto law [36] (Equation (2))

$$\tau = \tau_{max} \cdot \left(1 - e^{-j/K}\right), \tag{2}$$

where j is the shear displacement of the terrain and K is the shear deformation parameter which represents the shear displacement required for the development of the maximum shear stress. The maximum shear stress for a certain type of terrain is expressed by Mohr-Coulomb equation (Equation (3)) and depends on soil cohesion c and internal friction angle ϕ.

$$\tau_{max} = c + \sigma_n \cdot \tan\phi, \tag{3}$$

with σ_n bring the normal pressure (p in Bekker law). Values of the above mentioned empirical parameters k_{eq},c,ϕ and n can be found in the literature [37] for several terrain types. Also numerical methods for their real time determination have been developed [38]. These iterative algorithms allow to know some variable terrain characteristics during tracked machine motion. Focusing on tracked or wheeled vehicles on deformable terrain, the ϕ values for rubber-soil metal-soil contact are very similar to the soil internal friction angle. Adhesion values between rubber and soil or metal and soil differ from cohesion values [39]. If a shearing action is exerted on the soil by a track or a wheel, shear displacement of the terrain occurs. The shear displacement j is equivalent to the relative motion between track and soil (slip). As discussed in the following sections, the traction force developed by a tracked machine coincides with the integral of Equation (2) on the track area in contact with the soil. If no slip occurs no drawbar pull is developed. As shown in Figure 1 Janosi-Hanamoto law differs from experimental results in particular for compact terrains and high normal pressure [40]. Janosi-Hanamoto law expressed in Equation (2) is monotone increasing, whereas shear stress-shear displacement curves for dense frictional-cohesive soils exhibits a maximum [41]. To model a maximum in the shear stress—shear displacement behaviour other formulations are available in the literature [31].

$$\tau = \tau_{max} K_r \cdot \left[1 + \left(\frac{1}{K_r \cdot (1 - e^{-1})} - 1\right) \cdot e^{(1 - j/K_W)}\right] \cdot \left(1 - e^{-j/K_W}\right), \tag{4}$$

where K_r represents the ratio between the residual shear stress and its maximum admissible value while K_w represents the shear displacement at which the maximum shear stress occurs.

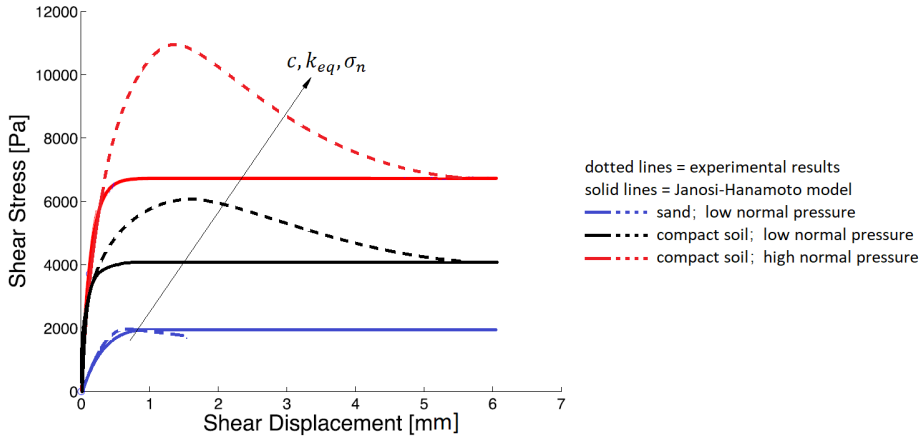

Figure 1. Janosi-Hanamoto model and experimental results, for different types of soil. Experimental data usually exhibit a peak in the traction capabilities for certain values of the shear displacement.

Equation (2) was implemented in the MTB model developed in this paper and also in other similar MTB models available in the literature [19]. As discussed, the application of this equation can be justified for loose soils and low normal pressure values. In the present MTB model Equation (2) was

also used for compact agricultural terrain due to the limited normal pressure on the soil exerted by the small size tracked vehicle. Focusing on the interaction of a cutting surface as a blade or a grouser with the soil, passive earth failure must be considered. In fact, the terrain in front of the cutting blade or behind the grouser can be brought in state of passive failure, due to the applied force [37]. According to Mohr criterion the passive failure of a soil prism occurs when the principal stress σ_p on its vertical sides is reached (Figure 2).

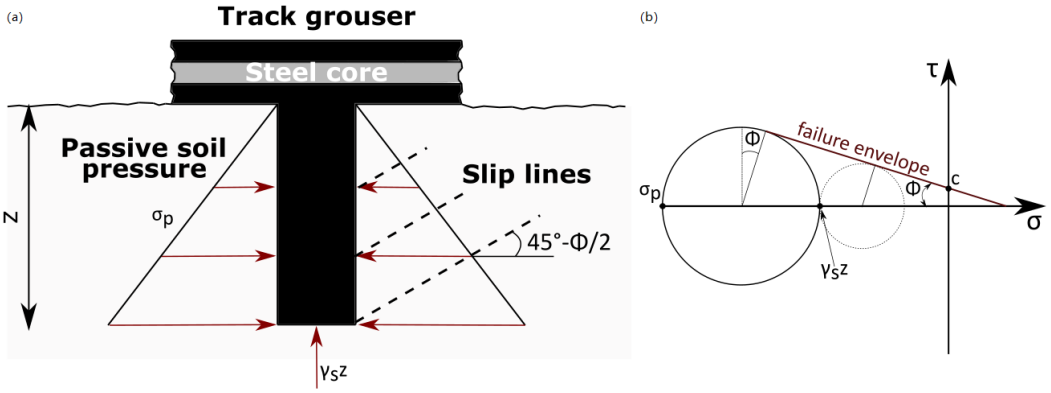

Figure 2. (**a**) Soil prism under passive compression; (**b**) Mohr circle.

Since the major principal stress is horizontal, failure of the soil prism takes place on slip lines sloped at $(45° - \phi/2)$.

Integrating the principal passive earth pressure σ_p on the grouser vertical area (Figure 3) the horizontal force acting on the lug can be determined (Equation (5)). It is the contribution to the vehicle traction force offered by a single grouser sunk into the soil.

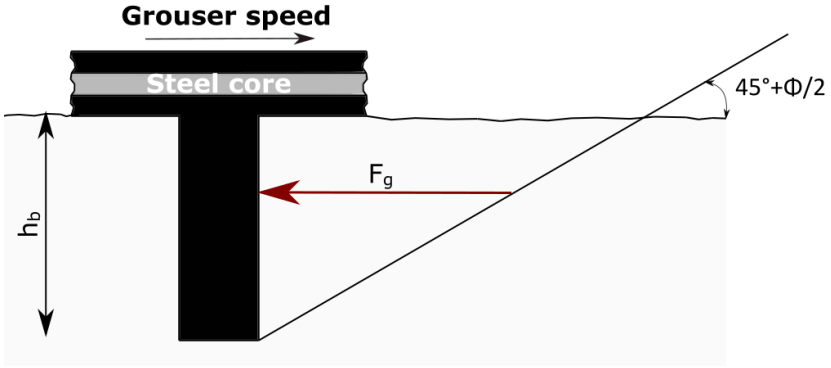

Figure 3. Interaction of a grouser with the terrain.

$$F_g = b\int_0^l \sigma_p dz = b\int_0^{h_b}\left(\gamma_s z N_\phi + 2c\sqrt{N_\phi}\right)dz = b\left(\frac{1}{2}\gamma_s h_b^2 N_\phi + 2ch_b\sqrt{N_\phi}\right), \quad (5)$$

in which γ_s is the specific weight of the soil, h_b is the grouser height sunk into the soil and N_ϕ is equal to $\tan^2(45° + \phi/2)$. If there is a normal pressure q acting on the terrain surface behind the grouser the resultant force is:

$$F_g = b\left(\frac{1}{2}\gamma_s h_b^2 N_\phi + qh_b N_\phi + 2ch_b\sqrt{N_\phi}\right). \quad (6)$$

It has to be pointed out that the passive earth pressure approach should be integrated also considering the existence of friction and adhesion on grouser vertical sides. Furthermore because

of the existence of shear stress at grouser-soil interface the normal pressure considered is no more a principal stress and the vertical surface of a grouser can be inclined with respect to the horizontal plane of the terrain. Reference [34] proposed a mathematical solution to correctly evaluate the force applied by a grouser taking into account its inclination and the presence of shear stress on its sides. Bekker proposed an equation based on an elastic stress distribution into the soil in order to consider the traction force developed by the vertical shear areas of a grouser. In Reference [42], Reece proposed a different equation based on static equilibrium to consider the same contribution. He formulated an equation of the total traction force given by a grouser considering the latter as a cutting surface and referring to a failure state of the soil.

3. Methods: Multibody Modelling

The MTB model of the tracked vehicle was built into the MSC ADAMS® (Newport Beach, CA, USA) software. Modelling of the tracks and the tensioning system was combined with a simplified body representing the main machine geometries. However, the mass and moments of inertia were estimated accordingly to the vehicle characteristics of a real machine for farming applications taken as a reference (see Table 1). Each track was made of 40 rigid bodies (links). The sprocket teeth transmit the motion by inserting into the links holes. The lateral movement of the track was bound with respect to the idle wheel by the central rail formed by each track segment (Figure 4).

Table 1. Main characteristics of the tracked vehicle.

Vehicle Properties	
Mass	750 kg
Length	1500 mm
Width	700 mm
Height	1130 mm
Track width	180 mm
Top speed	4 km/h

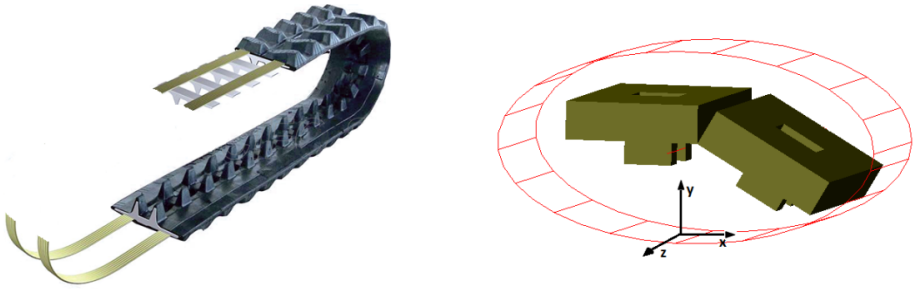

Figure 4. (**a**) Track structure, (**b**) links connected by a bushing element.

Small size tracked machines are usually equipped with rubber tracks. They have a steel core which gives a greater tensile strength. To obtain a track model with behaviour and properties similar to a real rubber track it was necessary to properly model the joints between consecutive links. In this work a bushing element was considered (Figure 4b). Three-dimensional bushing joints allowed to transmit elastic and damping forces and torques between two consecutive links. The required stiffness and damping coefficients were defined applying specific loads and comparing the virtual track behaviour with a reasonable response of a real one. In particular, a static test as the one shown in Figure 5 was simulated to see if the tensioning force and the proposed parameters for the bushing elements were coherent with the deflection of a track with a mass of 20 kg placed in between the idle wheel and the sprocket. Stiffness values are listed in Table 2.

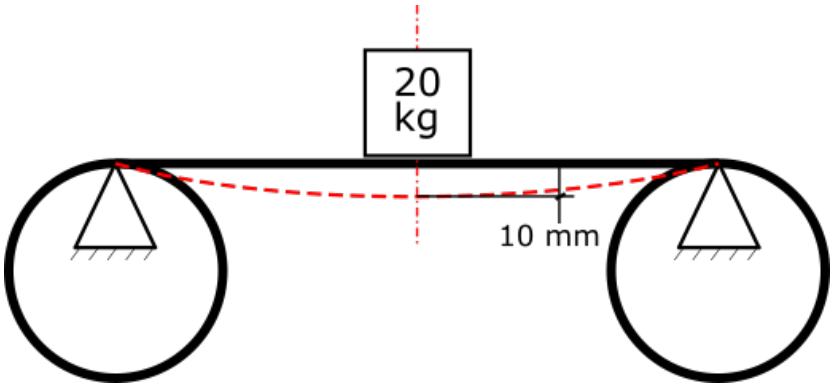

Figure 5. Deflection test.

Table 2. Bushing parameters.

	x	y	z
Translational Stiffness N/mm	10^4	10^4	10^4
Rotational Stiffness Nmm/deg	10^4	10^4	200

Negligible displacements and angular misalignments in x and y directions between two consecutive links were obtained using high translational and rotational stiffness values along those directions. Comparing the deformed shape of a real rubber track with the deformed shape of its MTB model, rotational stiffness in z direction was set. Track vibrations were limited by setting appropriate rotational damping in z direction, also considering rubber damping effect [43]. Idle wheels, driven wheels and oscillating plates with road-wheels were properly modelled (Figure 6). Contact forces were defined between each track link and each wheel. Low penetration depth and friction coefficient related to rubber-steel contact were defined. A damping value of 5.0 Ns/mm and a stiffness value of 100 N/mm were considered for the contact model of these elements. The driving wheel teeth insertion into links holes allowed torque transmission thanks to the contact force definition. In Figure 6 the position of the machine centre of mass (CM) is highlighted. Its position, as well as the overall moments of inertia of the vehicle are coherent with the vehicle characteristics shown before in Table 1.

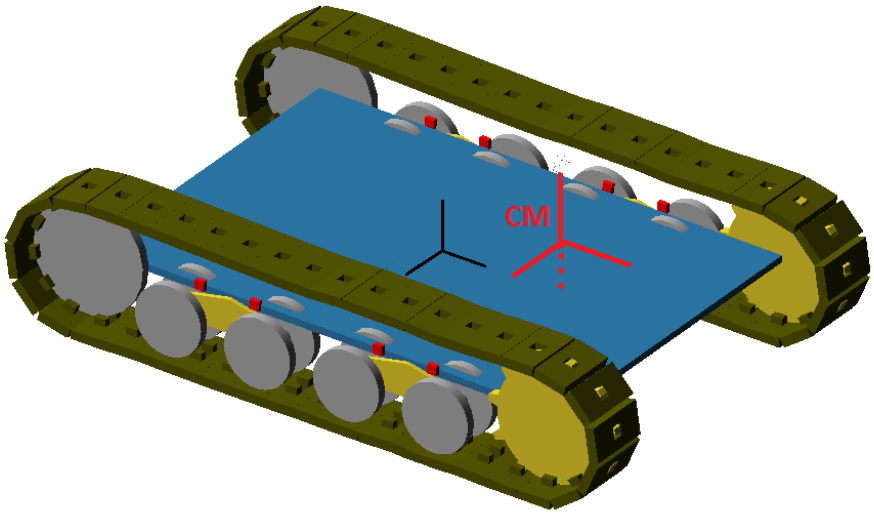

Figure 6. Complete model of the farming vehicle.

The track tensioning system was modelled so that the simultaneous rotation and translation of the idle wheel could be allowed (Figure 7). A translational joint was applied between a cubic pivot (dummy) body and the main body of the machine. The idle wheel was connected to the pivot body by means of a rotational joint. Considering typical tensioning force values for rubber tracks of small size machines, F force value (Figure 7) was set equal to 5100 N in such a way that the static track deformation would satisfy the test shown in Figure 5.

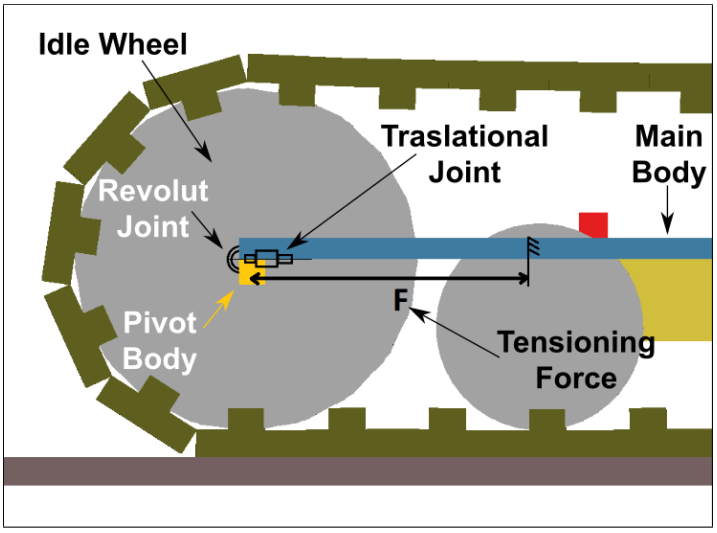

Figure 7. Tensioning system.

3.1. Deformable Ground Contact Model

The mathematical model of deformable soil was integrated into the MTB environment to correctly simulate the contact and the behaviour of the track on agricultural terrain. An efficient track-terrain contact model was developed implementing soil mechanics equations within routines defining different force elements applied to each rigid link of the track. Resulting forces acting on a link depend on ground characteristics, although they do not affect soil body deformation. The following routines description refers to smooth tracks (without grousers). Bekker equation Equation (1) was implemented in the routine related to sinkage behaviour of track links. The soil was modelled as a rigid body which may present irregularities such as peaks or valleys. Equation (1) multiplied for the link contact area was implemented in a non-linear Single-component-force (S-force) applied to the center of mass of each link and moving together with it (Figure 8). Thus each track link correctly sank into the ground body. The routine was defined to solve the Bekker force equation only when a contact between the soil body and the link was detected. The distance between the free surface of the soil and the contact base of a track link (y in Equation (1)) must be known at each time step of the solution. The terrain was modelled in the MTB environment as a rigid body with the desired shape to replicate the real undeformed one. To solve the contact equations, the information of the undeformed shape of the terrain was taken into account using a particular modelling strategy. A set of small and with low mass spheres forced to move with each track links but free to follow normally the terrain profile was used. The spheres CM position was evaluated at each time step, thus the information of the terrain geometry was available to the developed routine.

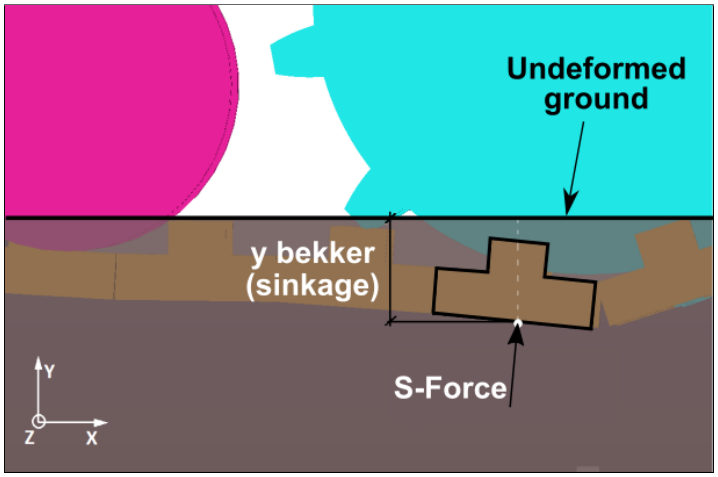

Figure 8. Bekker force acting on a single-track link.

The sinkage value y was constantly given as the difference between the base of the track link and the lowest contact point of each sphere (function of the sphere CM position and its radius). In other words, the marker centred in the sphere CM was one side of the non-linear spring defined by Equation (1) and applied to the track link surface. As a result, the tracks sinkage and the machine position depended on the terrain characteristics and shape (Figure 9).

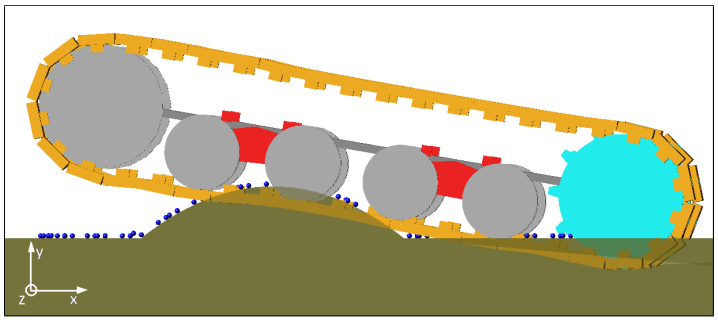

Figure 9. Auxiliary spheres following the undeformed shape of the terrain profile.

To be sure to not interfere with the track link movement, but to correctly sense the terrain shape, a frictionless contact model was implemented between each sphere and the ground body. Each sphere had to be vertically aligned with the corresponding link. For this reason, two motion laws were imposed. The first (between each sphere and the corresponding link), had a constant null displacement in z direction, and no constraints in the other directions. In the second motion law (between each sphere and the terrain) the sphere speed value in horizontal direction was set to be equal to the corresponding track link speed in the same direction. Soil damping was considered into account using typical values of terrain damping coefficients [44] and modifying Bekker equation as follows.

$$F = A\left(\frac{k_c}{b} + k_\phi\right) y^n + Ac\dot{y} = Ak_{eq}y^n + Ac\dot{y}. \tag{7}$$

The complete algorithm can be summarized as in Figure 10 in which F_B and F_t are the Bekker force and the traction force respectively.

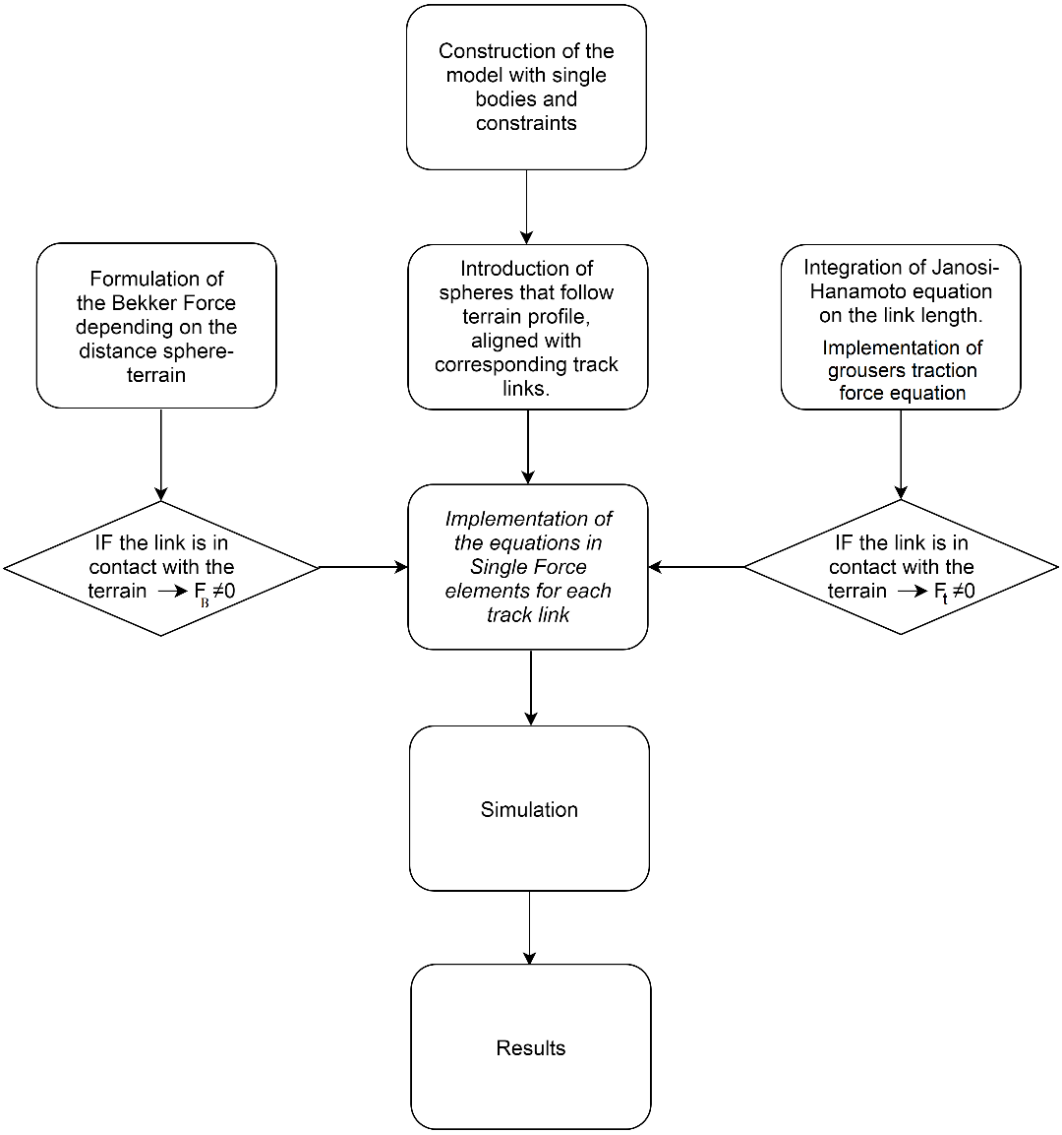

Figure 10. Complete multibody (MTB) code scheme

The contribution of each track portion in terms of traction force was obtained employing Janosi-Hanamoto equation in a specific routine inserted in another Single-component-force (S-force) defined for each track link. The internal shear stress – shear displacement law is reported below.

$$\tau = \tau_{max} \cdot \left(1 - e^{-j/K}\right) = (c + p(x) \tan \phi) \cdot \left(1 - e^{-j/K}\right) \tag{8}$$

As explained in Section 2, Equation (8) was implemented both for loose soil and compact agricultural terrain. Shear displacement j can be defined as the product ix, being

$$i = \frac{v_t - v}{v_t} = \frac{v_j}{v_t}. \tag{9}$$

i is also known as slip coefficient, v_t is the theoretical speed of the vehicle, v is the actual one and v_j is the relative speed between track portion and soil. In other words, v_j is the absolute link speed in x direction: when no slip occurs the track link in contact with the terrain is still. In this approach, the x coordinate is correctly identified as in Figure 11 and the theoretical speed is defined by Equation (10)

$$v_t = \omega_{sprocket} \cdot \left(r_{sprocket} + s_{track} \right). \quad (10)$$

$\omega_{sprocket}$ and $r_{sprocket}$ are the angular speed and the radius of the driven wheel, respectively, and s_{track} is the track thickness.

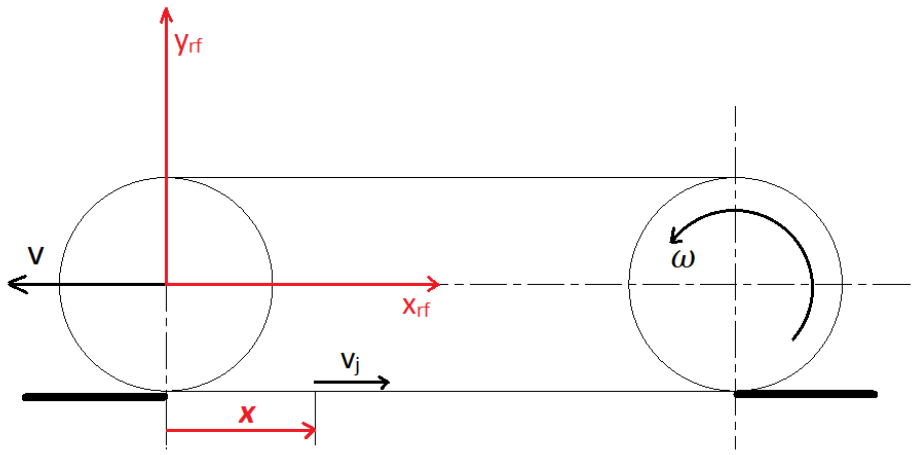

Figure 11. Coordinate system for traction force equation integration.

The syntax of the traction force was written into a specific routine which solved it only if contact between soil body and links was detected. The traction force expression was obtained integrating Equation (8) along the length of each track link, for the portion of the track in contact with the soil.

$$F = l \int_{b_1}^{b_2} (c + p(y) \tan\phi) \cdot \left(1 - e^{-ix/K}\right) dx = A\,(c + p(y) \tan\phi) \left[1 + \frac{K}{ib}\left(e^{-ib_1/K} - e^{-ib_2/K}\right)\right], \quad (11)$$

where A was the link base area, b was the link length and b_1 and b_2 were the limits of integration for a single link (Figure 12). They were moving limits of integration because the x coordinate was referred to the moving reference frame centred on the front idle wheel. Each link varied its position with respect to the idle wheel during vehicle motion as shown in Figure 11. The traction force routine was implemented into each link S-force element (Figure 12). Traction force sign was always opposite to the sign of the corresponding link speed (slip speed) coherently to the machine movement. The product between the normal pressure and the link contact area (term $Ap(y)$ in Equation (11)) coincided with the Bekker force previously implemented. Within the traction force formulation, the term $Ap(y)$ was replaced by the Bekker force definition. In this way the traction force evaluation depended on the current normal pressure under the track link (influenced by the terrain shape) and the approximation of the normal pressure with the overall average one was avoided. To sum up, soil mechanics equations were implemented only within force elements applied to the track links. No other equations related to soil stress and deformation were computed during simulations. However, tracks sinkage and developed drawbar pull were always related to deformable terrain characteristics and shape by mean of moving spheres constrained to each link as shown in Figure 12, where the sphere A is the sphere corresponding to the highlighted link.

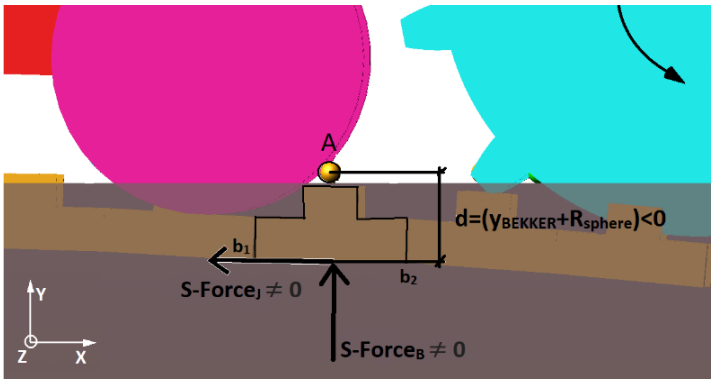

Figure 12. Forces acting on the single link.

3.2. Grousers Modelling

In order to evaluate the drawbar pull developed by a tracked machine the contribution in terms of traction force offered by grousers must be considered. The traction force equation presented in the previous section, and implemented for each track link, considered only the shear stress between the track flat surface and the soil. Focusing on rubber tracks with lugs, the cutting action of grousers sunk into the soil must be considered. In fact, grousers generate a greater traction effort contribution. This contribution varies with soil characteristics and grousers number and dimensions. In the presented model grousers as large as the track and 25 mm height were considered, one for each link.

For the sake of simplicity, no new rigid bodies were introduced into the MTB model and the link shape was not modified to include the grousers. The virtual grouser position is shown in Figure 13. Traction and Bekker force equations referred to a single grouser were properly related to its size, even if grouser body was not geometrically modelled. Fg in Figure 14 indicates the traction force developed by a grouser. The sinkage behaviour of the whole track changes with the presence of grousers because they are the first parts coming into contact with the soil. No new force elements were introduced but Bekker equation referred to the grouser base was introduced in the force formulation previously written for each link. If the base of the grouser sinks into the ground but the latter does not touch the link base, the track portion receives an upward force equal to:

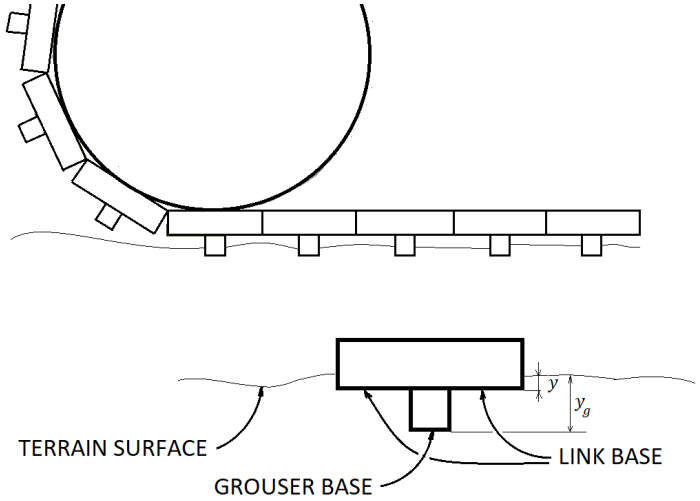

Figure 13. Virtual grouser position.

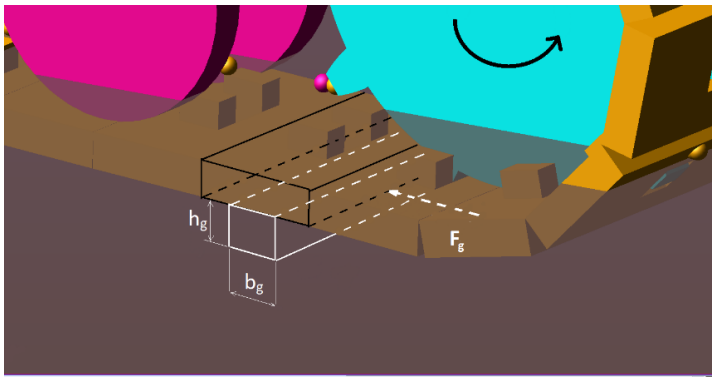

Figure 14. Grousers shape and position.

$$F_B = A_g \left(\frac{k_c}{b} + k_\phi \right) \cdot y_g^n + A_g c \dot{y}_g = A_g k_{eq} y_g^n + A_g c \dot{y}_g, \tag{12}$$

in which A_g is the grouser base area (Figure 13). If also the link base sinks into the soil the track portion receives an upward force equal to:

$$F_B = A_{link} k_{eq} y^n + A_{link} c \dot{y} + A_g k_{eq} y_g^n + A_g c y_g^n, \tag{13}$$

in which A_{link} is the link base area (Figure 13); y_g differs from y by the grouser height. Also, for the traction force developed by grousers no new force elements were introduced into the MTB model. The expression of the new force contribution was integrated into the existent traction force routine implemented for each track link. The resultant equation was a parametric equation in which grousers number and dimensions could be changed. The traction force offered by a grouser is related to the passive soil pressure and expressed by Equation (6), where q is different from zero only if the link base touches the soil. In fact, it represents the surcharge acting on the terrain surface portion under the grouser. For this reason, it can be set equal to the Bekker pressure acting on the link base. The grouser height sunk into the soil h_b depends on soil characteristics and Bekker equation. To sum up, the whole traction force equation implemented on each link force element depended on two contribution: the shear stress between link and/or grouser base and soil, and the grousers cutting action. If the whole grouser sank into the terrain and the latter touches the link base, the traction force expression for the link is reported in Equation (14).

$$F_t = A \left(c + p(y) \tan \phi \right) \cdot \left[1 + \frac{K}{ib} \left(e^{-ib_1/K} - e^{-ib_2/K} \right) \right] + F_g \left(1 - e^{-i\bar{x}/K} \right)_{q \neq 0}, \tag{14}$$

where A is the total link base area (which includes the grouser base area) and y_g is reasonably approximated with y values. If only part of the grouser sank into the soil, the traction force expression for the link which the grouser was attached to was expressed as in Equation (15).

$$F_t = A_g \left(c + p(y_g) \tan \phi \right) \cdot \left[1 + \frac{K}{ib} \left(e^{-ib_1/K} - e^{-ib_2/K} \right) \right] + F_g \left(1 - e^{-i\bar{x}/K} \right)_{q=0}. \tag{15}$$

The grouser traction force F_g was multiplied by the term $\left(1 - e^{-i\bar{x}/K} \right)$, in which $\bar{x}$ is the x coordinate value of the link CM marker. In fact, if no slip (i) was observed, grouser traction force contribution was null because no compressive stress was exerted on the soil portion behind the grouser. On the contrary, if slip value increased the grouser traction force contribution value rapidly tended to F_g. In fact, the initial phase of traction force generation in compressible terrain is soil compression by grousers in the x direction, which divides the soil under a track into separate blocks. This compression increases at least to the transition point, when a block is sheared off and starts sliding along the channel formed by the preceding grouser [45]. Furthermore, passive soil pressure is related to a state

of incipient plastic flow of the soil. The following Table 3 resumes the nomenclature adopted to explain the construction of the routine implemented into the MTB code.

The algorithm of the routine related to the traction and Bekker forces for a single-track link with grouser is summarized in Figure 15.

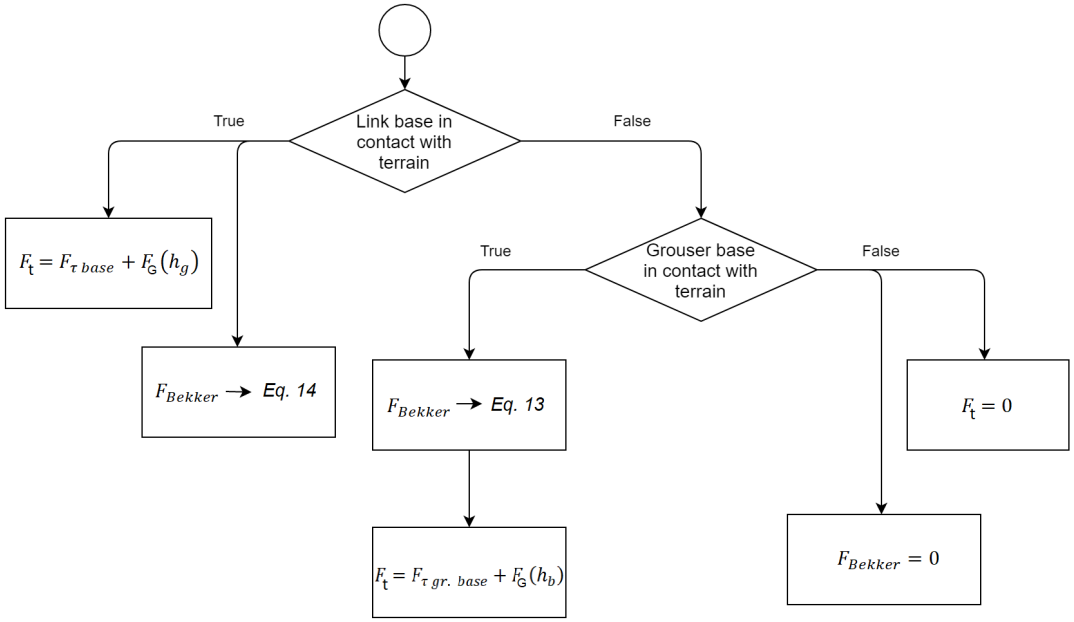

Figure 15. Evaluation strategy for the forces acting on each track link with grouser.

Table 3. Grousers MTB routine nomenclature.

Symbol	
h_g	Grouser height
h_b	Grouser height sunk into the soil
$F_{\tau gr,base}$	Traction force related to Janosi-Hanamoto law (first term of Equation (15)) acting on the grouser base
$F_{\tau base}$	Traction force related to Janosi-Hanamoto law (first term of Equation (14)) acting on the total link base area (grouser base + link base)
$F_G(h_b)$	Traction force developed by a grouser, equal to $F_g\left(1 - e^{-i\bar{x}/K}\right)$
F_t	Total traction force developed by a track link.

4. Simulations and Results

In this section, performance of the tracked vehicle on deformable soil are discussed. Before implementing the moving ground contact model for deformable terrains, the MTB model of the vehicle was validated with tests performed assigning simple contact elements with coulomb friction between each track link and the soil body [43].

4.1. Smooth Tracks

After this first stage the mathematical model of deformable soil described before was implemented into the MTB environment. Results related to the sinkage and the traction force of the tracks without grousers are reported. Changing accordingly the values of the constants k_{eq}, c, K and ϕ previously explained two different types of terrain (sand and agricultural soil) were simulated.

4.1.1. Normal Pressure Distribution and Track Sinkage

The same test was performed on sand and compact ground. Selecting the same location on the ground body (rigid), it was possible to evaluate different track deformation and sinkage for the two types of soil. The highest sinkage reached on sand was equal to 50 mm, whereas the maximum sinkage value on compact agricultural terrain was equal to 8 mm, because of the higher equivalent stiffness. Dividing the Bekker force values acting on each track link by its base area the pressure distribution both for sand and compact soil was obtained (Figure 16). A linear pressure distribution was also plotted to simply show the influence of the CM position and modifying the simplified assumption of constant pressure under tracks proposed in Reference [37].

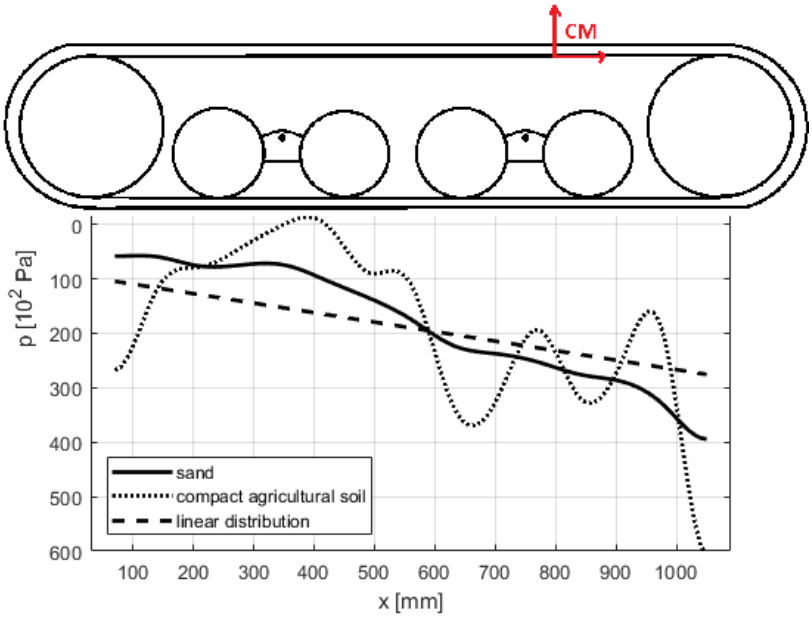

Figure 16. Pressure distribution for the track-terrain contact.

As shown in Reference [46], local rise of the pressure distribution is obtained at road-wheel locations. Moreover, pressure maxima values were grater for a compact terrain, as reported by Reference [37]. The mean value of normal pressure increased along x coordinate according to CM position. Local pressure peaks were also read under each grouser base, due to the grater sinkage of the latter with respect to the corresponding link base.

4.1.2. Traction Force-Slip Curves

Traction force-slip curves evaluated within the MTB code for smooth tracks are reported in Figure 17. Also, analytical curves evaluated both for sandy and compact terrain are presented and compared with MTB results. The only contribution to the traction effort derives by the shearing action between tracks and soil. To measure traction force and slip into the MTB environment, a spring force element was applied between the rear part of the vehicle and a fixed reference frame and the same increasing torque ramp was applied to the sprockets. The traction force as a function of time (linearly increasing with machine displacement) was read from the spring element. Slip as a function of time was evaluated as $i = 1 - v/v_t$. The two entities were then reported on the same plot (Figure 17).

The maximum traction force value reached on compact agricultural soil was greater than the traction force value on sand, mainly due to higher ϕ and c values.

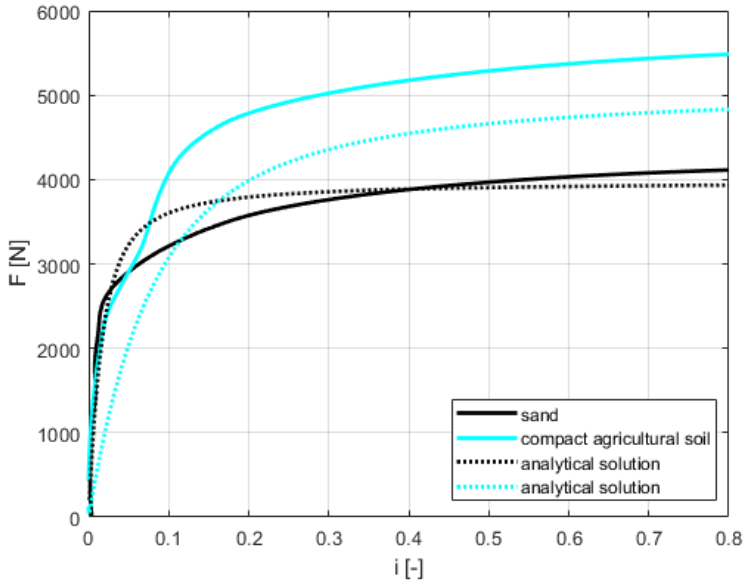

Figure 17. Traction force-slip curves.

4.2. Tracks with Grousers

Results in term of drawbar pull and sinkage for complete tracks model with grousers are reported. Comparison with results obtained with smooth tracks is also pointed out.

4.2.1. Sinkage

On soft sandy terrain 12 mm height grousers completely sank into the soil, due to ground characteristics and machine weight (Figure 18a).

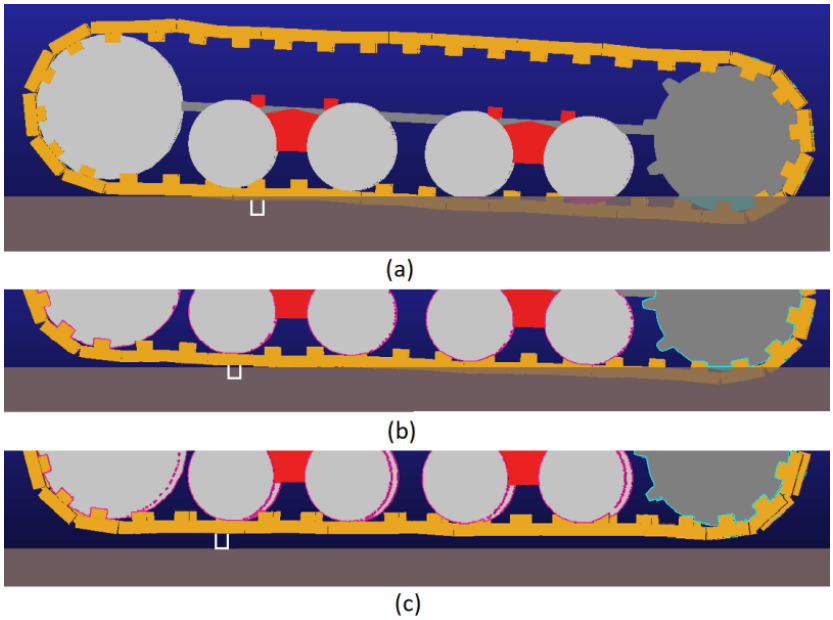

Figure 18. Tracks sinkage with 12 mm high grousers on sand (**a**), 25 mm high grousers on sand (**b**), and 25 mm high grousers on compact terrain (**c**). In each figure, only one virtual grouser is represented on each image to figure out the track sinkage.

With 25 mm height grousers the global vehicle sinkage was slightly smaller (Figure 18b), according to Bekker force acting on grousers base area. On compact agricultural soil grousers partially

sank into the ground, but the latter did not come into contact with track links base (Figure 18c). Figure 18a–c highlight just one grouser for the sake of clarity. However as discussed before, simulations take into account the effects from all the grousers of the tracks.

4.2.2. Traction Force-Slip Curves

The grousers action contribution to the traction effort is reported and discussed. The procedure to obtain traction force-slip curves in MTB model was the same reported in Section 4.1.2. Traction force developed by tracks with grousers was investigated for two different types of soil: sand and compact agricultural terrain. The effect of grousers height was also highlighted. The maximum traction force value was reached on sand with 25 mm height grousers (Figure 19). It was about 250% of the value reached with smooth tracks (on sand). Comparing the results obtained for different grouser height on sand (12 mm and 25 mm), it is clear that the variation of traction force maximum values was not proportional to grousers height variation. The mean term of Equation (6) reported below is proportional both to grouser height sunk into the soil (h_b) and surcharge q. Moreover, it is about 100 times greater than other two terms. The height of the grouser part sunk into the soil (h_b) on sand was almost equal to the total grouser height, both for 25 mm and 12 mm grousers height (Figure 18). On the contrary pressure q exerted by links bases was greater for 12 mm height grousers on sand, due to the greater global sinkage. For this reason, maximum traction effort reached with 12 mm height grousers was about 80% of the value referred to 25 mm height grousers (Figure 19).

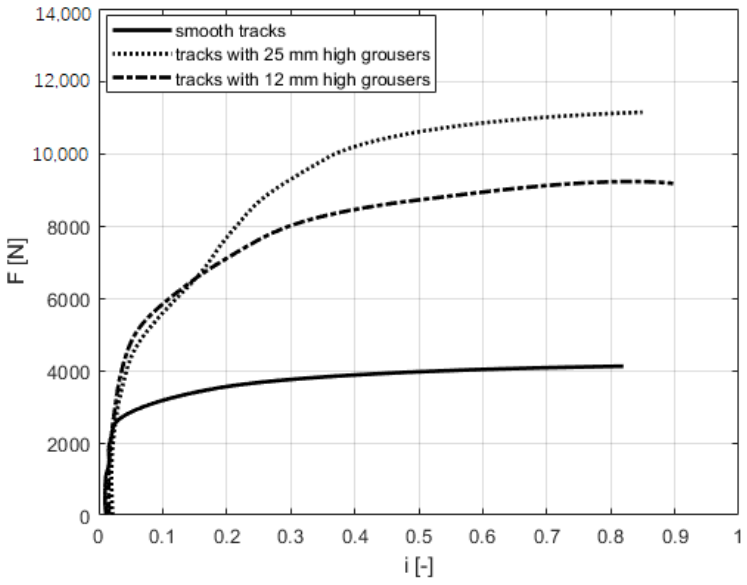

Figure 19. Traction force-slip curves on sand.

On compact agricultural soil the maximum value of the traction force was smaller than the value reached with smooth grousers (Figure 20). Grousers contribution in terms of traction effort is limited, because soil stiffness does not allow them to sink. Shearing action between tracks and terrain had the main role in drawbar pull development, but the sum of the grousers shear base areas is smaller than the total area of smooth tracks.

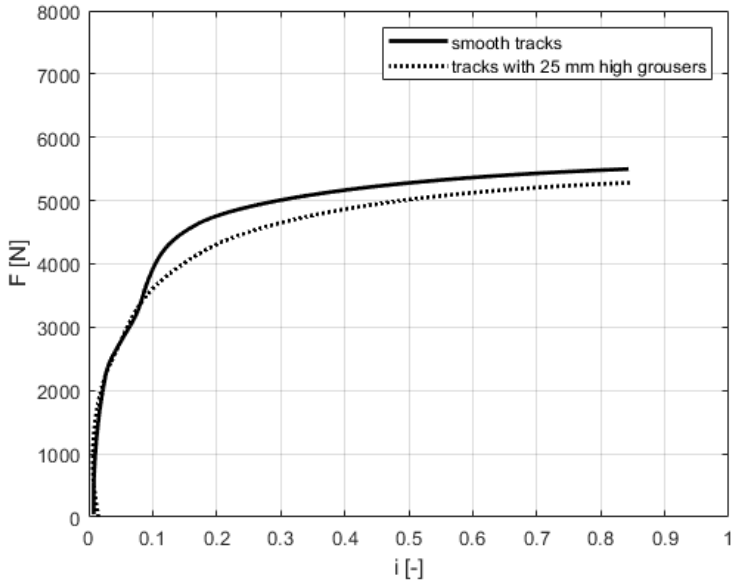

Figure 20. Traction force-slip curves on soil.

5. Discussion and Conclusions

A multibody model of a tracked vehicle for off-road application is presented. A specifically designed algorithm to model track-deformable terrain interaction was developed. Bekker and Janosi-Hanamoto soil mechanics equations were implemented to properly simulate both sinkage and traction behaviour of the tracked machine. Moreover, a passive earth failure model was adopted to also consider the contribution of grousers in terms of drawbar pull. The two flexible tracks were modelled as groups of rigid links constrained by bushing elements able to replicate the elastic behaviour of the track. On each track link, Single component Force elements were applied and related to the soil mechanics equation solved only for those links in contact with the terrain. The use of small rigid spheres kinematically constrained to the link motion, allowed to have at each integration step the local shape of the terrain body in contact with their corresponding link. A simple terrain modelling procedure was adopted to obtain indicative results about tracked vehicles behaviour on deformable soil, in favour of computational times. Vehicle sinkage, developed traction force and pressure distribution under tracks on different type of soil were highlighted in the presented results. The type of terrain was varied into the MTB environment changing the soil characteristic coefficients. In particular, traction force-slip curves were compared with the analytical ones and good agreement is shown. Pressure peaks under road-wheels were correctly evaluated and the actual pressure under each links contributed to the overall traction force computation. Drawbar pull developed by smooth tracks on different type of soil was compared with drawbar pull developed by tracks with grousers. The influence of grousers height and contact surface amplitude was also analysed highlighting the higher impact in traction force on soil when compared with smooth links. As expected, a much smaller impact of the grousers on compact terrain model was highlighted due to the limited sinkage.

Author Contributions: Conceptualization, F.M., A.S. and A.N.; methodology, F.M., A.S. and A.N.; software, F.M. and A.N.; validation, F.M., A.S. and A.N.; formal analysis, F.M. and A.N.; investigation, F.M., A.S. and A.N.; data curation, F.M. and A.N.; writing—original draft preparation, F.M. and A.N.; writing—review and editing, F.M., A.S. and A.N.; visualization, F.M., A.S. and A.N.; supervision, A.S.; project administration, A.S. All authors have read and agreed to the published version of the manuscript.

Funding: This research received no external funding

Conflicts of Interest: The authors declare no conflict of interest.

References

1. Blundell, M.; Harty, D. *The Multibody Systems Approach to Vehicle Dynamics*, 2nd ed.; Butterworth-Heinemann: Oxford, UK, 2014.
2. Pascuzzi, S. A multibody approach applied to the study of driver injuries due to a narrow-track wheeled tractor rollover. *J. Agric. Eng.* **2015**, *46*, 105–114. [CrossRef]
3. Melzi, S.; Sabbioni, E.; Vignati, M.; Cutini, M.; Brambilla, M.; Bisaglia, C.; Cavallo, E. Multibody model of fruit harvesting trucks: Comparison with experimental data and rollover analysis. *J. Agric. Eng.* **2015**, *49*, 92–99. [CrossRef]
4. Yong, R.N. Track-soil interaction. *J. Terramech.* **1984**, *21*, 133–152. [CrossRef]
5. Pacejka, H.B. *Tyre and Vehicle Dynamics*; Butterworth-Heinemann: Oxford, UK, 2002.
6. Bekker, M.G. *Theory of Land Locomotion*; University of Michigan Press: Ann Arbor, MI, USA, 1962.
7. Wong, J.Y.; Preston-Thomas, J. On the characterization of the shear stress-displacement relationship of terrain. *J. Terramech.* **1982**, *19*, 225–234. [CrossRef]
8. Wong, J.Y. Data processing methodology in the characterization of the mechanical properties of terrain. *J. Terramech.* **1980**, *17*, 13–41. [CrossRef]
9. Taheri, S.; Sandu, C.; Taheri, S.; Pinto, E.; Gorsich, D. A technical survey on terramechanics models for tire–terrain interaction used in modeling and simulation of wheeled vehicles. *J. Terramech.* **2014**, *57*, 1–22. [CrossRef]
10. Wong, J.Y. Some recent developments in the computer-aided methods for design evaluation of off-road vehicles. *Proc. Symp. Transp. Syst.* **1990**, *28*, 269–288.
11. Wong, J.Y. On the study of wheel-soil interaction. *J. Terramech.* **1984**, *21*, 117–131. [CrossRef]
12. Senatore, C.; Iagnemma, K. Analysis of stress distributions under lightweight wheeled vehicles. *J. Terramech.* **2013**, *51*, 1–17. [CrossRef]
13. Shabana, A.A. ANCF Tire Assembly Model for Multibody System Applications. *J. Comput. Nonlinear Dyn.* **2015**, *10*, 024504. [CrossRef]
14. Patel, M.; Orzechowski, G.; Tian, Q.; Shabana, A.A. A New Multibody System Approach for Tire Modeling Using ANCF Finite Elements. *Proc. Inst. Mech. Eng. Part K J. Multi Body Dyn.* **2016**, *230*, 69–84. [CrossRef]
15. Sivo, S.; Stio, A.; Mocera, F.; Somà, A. A study of a rover wheel for Martian explorations, based on a flexible multibody approach. *Proc. Inst. Mech. Eng. Part J. Multi Body Dyn.* **2019**, *234*, 306–321. [CrossRef]
16. Reece, A.R. Principles of soil-vehicle mechanics. *Proc. Inst. Mech. Eng. Automob. Div.* **1965**, *108*, 45–66. [CrossRef]
17. Harnisch, C.; Lach, B.; Jakobs, R.; Troulis, M.; Nehls, O. A new tyre–soil interaction model for vehicle simulation on deformable ground. *Veh. Syst. Dyn.* **2005**, *3*, 384–394. [CrossRef]
18. Sharaf, A.M.; Rahnejat, H.; King, P.D. Analysis of handling characteristics of all-wheel-drive off-road vehicles. *Int. J. Heavy Veh. Syst.* **2008**, *15*, 89–106. [CrossRef]
19. Rubinstein, D.; Hitron, R. A detailed multibody model for dynamic simulation of off-road tracked vehicles. *J. Terramech.* **2004**, *41*, 163–173. [CrossRef]
20. Madsen, J., Heyn, T.; Negrut, D. *Methods for Tracked Vehicle System Modelling and Simulation*; Technical Report 2010–01; Department of Mechanical Engineering, University of Wisconsin: Madison, WI, USA, 2010.
21. Frimpong, S.; Thiruvengadam, M. Contact and joint forces modeling and simulation of crawler-formation interactions. *J. Powder Metall. Min.* **2015**, *4*, 1–14. [CrossRef]
22. Frimpong, S.; Thiruvengadam, M. Rigid multi-body kinematics of shovel crawler-formation interactions. *Int. J. Mining Reclam. Environ.* **2016**, *30*, 347–369. [CrossRef]
23. Baik, D.K. *Systems Modeling and Simulation: Theory and Applications*; Springer: Jeju Island, Korea, 2005; pp. 553–558.
24. Matej, J. Tracked mechanism simulation of mobile machine in MSC.ADAMS/View. *Res. Agric. Eng.* **2010**, *56*, 1–7. [CrossRef]
25. Liu, C.H.; Wong, J.Y.; Mang, H.A. Large strain finite element analysis of sand: Model, algorithm and application to numerical simulation of tire-sand interaction. *Comput. Struct.* **1999**, *74*, 253–265. [CrossRef]
26. Krenn, R.; Hirzinger, G. Simulation of rover locomotion on sandy terrain-modeling, verification and validation. In Proceedings of the 10th ESA Workshop on Advanced Space Technologies for Robotics and Automation—ASTRA 2008, Noordwijk, The Netherlands, 11–13 November 2018.

27. Gao, Y.; Wong, J.Y. The development and validation of a computer aided method for design evaluation of tracked vehicles with rigid links. *Proc. Inst. Mech. Eng. Part D J. Automob. Eng.* **1994**, *208*, 207–215. [CrossRef]
28. Nakanishi, T.; Shabana, A.A. Contact forces in the non-linear dynamic analysis of tracked vehicles. *Int. J. Numer. Methods Eng.* **1994**, *37*, 1251–1275. [CrossRef]
29. Omar, M.A. Modular multibody formulation for simulating off-road tracked vehicles. *Stud. Eng. Technol.* **2014**, *1*, 77–100. [CrossRef]
30. Ryu, H.S.; Bae, D.S.; Choi, J.H.; Shabana, A.A. A compliant track link model for high-speed, high-mobility tracked vehicles. *Int. J. Numer. Methods Eng.* **2000**, *48*, 1481–1502. [CrossRef]
31. Bando, K.; Yoshida, K.; Hori, K. The development of the rubber track for small size bulldozers. *SAE Trans. Sect. 2 J. Commer. Veh.* **1991**, *100*, 339–347.
32. Bosso, N.; Spiryagin, M.; Gugliotta, A.; Somà, A. *Mechatronic Modeling of Real-Time Wheel-Rail Contact*; Springer: Berlin/Heidelberg, Germany, 2013.
33. Nicolini, A.; Mocera, F.; Somà, A. Multibody simulation of a tracked vehicle with deformable ground contact model. *Proc. Inst. Mech. Eng. Part K J. Multi Body Dyn.* **2019**, *233*, 152–162. [CrossRef]
34. Hettiaratchi, D.R.P.; Reece, A.R. The calculation of passive soil resistance. *Geotecnique* **1974**, *24*, 289–310. [CrossRef]
35. Wong, J.Y.; Garber, M.; Preston-Thomas, J. Theoretical prediction and experimental substantiation of the ground pressure distribution and tractive performance of tracked vehicles. *Proc. Inst. Mech. Eng. Part D J. Automob. Eng.* **1984**, *198*, 265–285. [CrossRef]
36. Janosi, Z.J.; Hanamoto, B. The analytical determination of drawbar pull as a function of slip for tracked vehicles in deformable soils. In Proceedings of the 1st International Conference on the Mechanics of Soil Systems, Torino, Italy, 12–16 June 1961.
37. Wong, J.Y. *Terramechanics and Off-Road Vehicles Engineering*, 2nd ed.; Butterworth-Heinemann: Oxford, UK, 2010.
38. Hutangkabodee, S.; Zweiri, Y.H.; Seneviratne, L.D.; Althoefer, K. Validation of soil parameter identification for track-terrain interaction dynamics. In Proceedings of the 2007 IEEE/RSJ International Conference on Intelligent Robots and Systems, San Diego, CA, USA, 29 October–22 November 2007.
39. Neal, M.S. Friction and adhesion between soil and rubber. *J. Agric. Eng. Res.* **1966**, *11*, 108–112. [CrossRef]
40. Jayakumar, P.; Melanz, D.; MacLennan, J.; Gorsich, D.; Senatore, C.; Iagnemma, K. Scalability of classical terramechanics models for lightweight vehicle applications incorporating stochastic modeling and uncertainty propagation. *J. Terramech.* **2014**, *54*, 37–57. [CrossRef]
41. Grecenko, A. Binomic slip-thrust equation for tractors in predominantly frictional soil. *J. Terramech.* **1967**, *4*, 37–54. [CrossRef]
42. Reece, A.R. The fundamental equation of earthmoving mechanics. In *Proceedings of the Institution of Mechanical Engineers, Conference Proceedings*; Sage: London, UK, 1964; Volume 179, pp. 16–22.
43. Mocera, F.; Nicolini, A. Multibody simulation of a small size farming tracked vehicle. *Procedia Struct. Integr.* **2018**, *8*, 118–125. [CrossRef]
44. Rubinstein, D.; Coppock, J.L. A detailed single-link track model for multi-body dynamic simulation of crawlers. *J. Terramech.* **2007**, *44*, 355–364. [CrossRef]
45. Grecenko, A. A Re-examined principles of thrust generation by a track on soft ground. *J. Terramech.* **2006**, *44*, 123–131. [CrossRef]
46. Keller, T.; Arvidsson, J. A model for prediction of vertical stress distribution near the soil surface below rubber-tracked undercarriage systems fitted on agricultural vehicles. *Soil Tillage Res.* **2016**, *155*, 116–123. [CrossRef]